Scanning Electrochemical Microscopy and Conductive Probe Atomic Force Microscopy Studies of Hydrogen-Terminated Boron-Doped Diamond Electrodes with Different Doping Levels

Katherine B. Holt and Allen J. Bard*

Department of Chemistry and Biochemistry, The University of Texas at Austin, Austin, Texas 78712

Yoshiyuki Show and Greg M. Swain

Department of Chemistry, 320 Chemistry Building, Michigan State University, East Lansing, Michigan 48824-1322

Received: April 23, 2004; In Final Form: June 28, 2004

The pattern of conductivity and electrochemical activity at the surfaces of hydrogen-terminated boron-doped diamond electrodes, with different boron doping levels, were measured using conductive probe atomic force microscopy (CP-AFM) and scanning electrochemical microscopy (SECM). CP-AFM showed that the surface was predominantly insulating, with discrete conducting areas of less than 2 μm in diameter, randomly and nonuniformly distributed on the surface. SECM imaging correlated these conductive areas with electrochemical activity and showed that the electrode surface was only partly electrochemically active and that the active area of the electrodes increased with boron doping level. Cyclic voltammograms and SECM approach curves obtained using $Ru(NH_3)_6^{3+/2+}$ as the redox mediator were characteristic of those obtained at partially blocked electrodes of nonuniform activity, or a microelectrode array. By use of this model, the SECM approach curves could be fit to obtain values of the fraction of the surface that was electrochemically active. The active area of the electrode was related to the boron doping level.

1. Introduction

Boron-doped diamond (BDD) thin films grown using chemical vapor deposition (CVD) techniques have in recent years been studied and characterized as an electrode material.[1−3] BDD is grown using a feed-gas mixture of 0.3−1.0% CH_4 in H_2, which can be activated using either a hot-filament or a microwave plasma source, and deposited on a suitable substrate, such as conducting silicon, at a substrate temperature of 700−900 °C.[4] The boron dopant is added to the source gas mixture, often in the form of diborane (B_2H_6), at concentrations ranging from 1,000 to 10,000 ppm. This results in the formation of a thin film of polycrystalline diamond with a thickness of 1−10 μm and a boron carrier concentration of 1×10^{20} cm^{-3} or greater. Film resistivities lower than 0.01 Ω cm are typical for such films. These films exhibit metallic conductivity and have many useful properties as an electrode material. BDD has a very low capacitive background current, making it useful in analytical applications where small concentrations of analyte can be detected.[2,4−7] It also has a wide potential window in aqueous solvent of up to 3 V, which allows electroactive species to be detected that may be masked by the solvent decomposition and surface reactions on other electrode materials. Other desirable properties, such as the intrinsic inert nature of diamond, as well as its hardness and robustness, lead to applications where electrode stability is important, such as in wastewater treatment.[8,9]

Although the above properties make BDD electrodes attractive for a range of applications, they still possess some characteristics that are not fully understood from a fundamental point of view. The principle among these is the mechanism of electron exchange between the diamond surface and solution redox species. Simple reversible and quasireversible redox couples, such as $Fe(CN)_6^{3-/4-}$, $Ru(NH_3)_6^{3+/2+}$, $IrCl_6^{2-/3-}$, $Fe(H_2O)_6^{3+/2+}$, and benzoquinone/hydroquinone exhibit electrochemical reduction and oxidation at BDD electrodes around the equilibrium potential of the redox couple, but with varying values of heterogeneous rate constant. The behavior of highly doped films is usually described as "metallic", suggesting that direct electron transfer can occur between the valence or conduction band of the electrode and the redox species. However, as the valence band of boron-doped polycrystalline diamond has been estimated to be at ~550 mV vs SCE,[10] with a 5.4 eV band gap between that and the conduction band and facile electron transfer is observed for the $Ru(NH_3)_6^{3+/2+}$ couple, whose formal potential occurs at −218 mV vs SCE (i.e., in the band gap), it is clear that direct electron exchange does not occur predominantly via either the conduction or the valence band. The electrochemical response has been explained in terms of electronic states present in the band gap at this potential, which mediate charge transfer.

The electronic properties of the BDD electrode are dependent on a complex range of factors: (a) dopant concentration and the resulting density of states (DOS); (b) structural defects in the diamond film; (c) nondiamond carbon impurity content (e.g., sp^2 inclusions); (d) crystallographic orientation; (e) surface termination (H, O); (f) fraction of grain boundaries. The biggest influence on the electrochemical properties of the diamond films is probably the concentration of boron dopant. During the growth process, the boron atoms substitutionally insert for carbon atoms and also accumulate at grain boundaries. In films of a low

* To whom correspondence may be addressed. E-mail: ajbard@mail.utexas.edu.

10.1021/jp048222x CCC: $27.50
Published on Web 08/27/2004

doping level (10^{17} cm^{-3}), the boron impurities form an acceptor band ~0.35 eV above the valence band. However, as the dopant level is increased to the $10^{19}-10^{20}$-cm^{-3} level, more commonly encountered for these films, there is mutual interaction between the boron centers and the impurity band broadens and shifts toward the valence band. Hence at low boron levels, conduction likely occurs by electron/hole hopping, whereas at higher concentrations, conduction may occur directly through the impurity band. It is found that ΔE_p for several redox couples decreases with increasing boron doping level[11,12] and that higher peak currents are observed as boron levels are increased. This is attributed to an increased density of electronic states formed within the band gap, as the boron level increases. However, this observation is counterintuitive in some ways, as carrier mobilities tend to *decrease* with increasing boron content, as more scattering occurs due to the presence of more boron impurity centers.

Several authors have investigated the mechanism of charge transfer at BDD electrodes, using a variety of electrochemical methods to extract the apparent heterogeneous rate constant for different redox couples.[1,11,13−18] However, the information obtained has been to some extent ambiguous and inconclusive, in part due to two factors: (1) an inconsistency in the literature as to the heterogeneous electron-transfer kinetics on BDD for couples showing reversible and quasireversible behavior, such as $Fe(CN)_6^{3-/4-}$, $Ru(NH_3)_6^{3+/2+}$, $IrCl_6^{2-/3-}$, $Fe(H_2O)_6^{3+/2+}$, and benzoquinone/hydroquinone, and in particular what constitutes a pure "outer-sphere" electron transfer at BDD. Although some couples, such as $Ru(NH_3)_6^{3+/2+}$ and $IrCl_6^{2-/3-}$, in general, exhibit apparent heterogeneous rate constants, k_{app}^0, within an order of magnitude of those observed at activated glassy carbon, in some cases, such as for benzoquinone/hydroquinone and Fe^{2+}/Fe^{3+}, the apparent rate constants obtained were found to be several orders of magnitude lower than those for other electrode materials. The reason for the sluggish kinetics for benzoquinone/hydroquinone is unknown but may be due to either the electronic properties of the electrode or complications in the reaction mechanism. The slow kinetics for the Fe^{2+}/Fe^{3+} couple has been suggested as due to a lack of surface carbonyl functionalities to catalyze the electron-transfer reaction.[19] Some redox couples, such as $Fe(CN)_6^{3-/4}$, which are traditionally treated as outer sphere behave anomalously at carbon-based electrodes and may change to an inner-sphere electron-transfer mechanism at diamond electrodes, where some degree of interaction occurs between the redox species and the electrode surface.[1,20] In these cases, factors such as the termination of the surface and presence of oxygen functionalities can influence the kinetics of the reaction. Several studies have investigated the kinetics of electron transfer at BDD electrodes using this couple and have treated the data assuming pure outer-sphere behavior, which may not in reality be the case. (2) A second factor that leads to confusion is the inconsistency in the quality of the BDD electrodes used to obtain the measurements. In particular, in many cases, the values of the apparent heterogeneous rate constant have been extracted from cyclic voltammetry experiments without any consideration of the resistance of the electrodes. As the quality and the doping level of the BDD electrodes vary, so too does the intrinsic conductivity of the diamond film. The deposition method, substrate material, and electrode-mounting technique are all variables, which if not carefully controlled, can lead to changes in resistivity between different samples. Resistance within the thin film electrodes will result in greater values of ΔE_p, which, if not accounted for, can be misinterpreted as a slower heterogeneous rate constant. Relatively slow kinetics have been reported even for true outer-sphere redox couples, such as $Ru(NH_3)_6^{3+/2+}$ and $IrCl_6^{2-/3-}$, whose rate constants should be largely independent of the nature of the electrode surface. The electrochemical behavior of boron-doped diamond has recently been discussed[1,18] in an attempt to standardize the behavior of high-quality polycrystalline electrodes. For the outer-sphere reversible reduction of $Ru(NH_3)_6^{3+}$, ΔE_p values of between 70 and 100 mV are typically recorded for highly doped "semimetallic" films. This is in contrast to the value of 59 mV expected for a reversible electron transfer, which is observed for this redox couple on platinum electrodes. As this electron transfer is relatively insensitive to surface structure,[19] the most important factor affecting the rate of reaction is then suggested to be the electronic properties of the electrode, and this in turn is dependent on the dopant concentration. How the dopant concentration affects the rate and mechanism of charge transfer is one of the questions this paper seeks to address.

The apparent heterogeneous rate constant for simple outer-sphere electron-transfer reaction at BDD electrodes has been discussed in several papers[1,11,13−17] and two general models for charge transfer have emerged. The first model is similar to that discussed above, where electron transfer is said to be mediated via impurity states present within the band gap,[1] and so the rate of the charge transfer is dominated by the available density of states. Such states arise due to the overlapping of wave functions of neighboring boron atoms and hence result in the formation of impurity bands. The rate of heterogeneous electron transfer will depend on the availability of states of the correct energy relative to the potential of the redox couple. The impurity bands are believed to have a large contribution from the presence of lattice hydrogen. In fact, van de Lagemaat et al.[17] suggest that interfacial states (at or near the surface) distributed in energy throughout the band gap mediate electron transfer between the valence band and the redox system at boron-doped single-crystal diamond electrodes. The surface states are speculated to be defects or impurity sites located very close to the surface, perhaps caused by hydrogen, boron, oxygen, or carbon inclusions, and are proposed to mediate exchange of the electrons between the valence band of the diamond and the redox system. Such an exchange takes place by multiple electron hopping. Heterogeneous kinetics are highly dependent on the rate of tunneling of electrons/holes to the redox species in solution; thus if deep boron dopant sites are involved in electron transfer, then the kinetics may be slow and limited by the rate at which the carrier can migrate to the surface. The electron-transfer rate will also be sensitive to the state of the surface interface. It is suggested that the heterogeneous rate constant is decreased at BDD electrodes in comparison to noble metals, due to a lower density of electronic states of an appropriate energy, coupled with slow charge transfer limited by the rate of migration of carriers to the surface. The available DOS and carrier migration will be dependent on dopant concentration. Thus, as the boron content is increased, a greater density of states may be available for electron transfer. However, an increase in boron impurity centers may lead to more scattering and hence a lower mobility of carriers.

The second model argues that polycrystalline boron-doped diamond surfaces exhibit heterogeneity in electron-transfer rates over the surface, due to nonuniform distribution of dopant throughout the diamond film. The surface may therefore consist of sites of fast (reversible) kinetics where the dopant level is high and sites of very slow kinetics (irreversible) where there is less dopant. It is known that boron incorporates into the

diamond structure in different concentrations depending on the crystal face of the diamond. The boron concentration in {111} growth sectors is five or more times greater than that found in {100} sectors.[21] Dopant may also accumulate at the sites of grain boundaries, crystal edges, and other defects, but these atoms are not expected to be electronically active. On the polycrystalline surface, different crystal faces are exposed, resulting in a heterogeneous electron-transfer rate that is an average value for the whole electrode area. Becker et al. studied diamond films with doping levels between 200 and 6000 ppm using cyclic voltammetry and electrochemical impedance spectroscopy.[13,14] They observed strong deviations from reversible charge transfer for "outer-sphere" reactions ($Fe(CN)_6^{3-/4-}$ and $Ru(NH_3)_6^{3+/2+}$). Limiting current densities that were lower than predicted and the existence of an additional capacitive element in the impedance spectra at higher frequencies led to the suggestion of a geometric surface-blocking model, where only limited areas of the diamond film are believed to be electrically conducting. Hence this model suggests that the rate of electron transfer is not limited by the migration of carriers to the electrode surface but more by the availability of active surface sites for electron transfer. These may be sites where boron dopant has accumulated and where conductive pathways are available through the film.

Both of these models suggest that the rate of heterogeneous electron transfer will depend on boron concentration within the film. However, as discussed above, the mechanism for electron transfer might be different at different doping levels. For example, an electron-hopping mechanism may dominate at low boron levels, whereas conduction via the impurity band or surface states may be the main mechanism at higher doping levels. This study uses the surface probe techniques of scanning electrochemical microscopy (SECM) and conductive probe atomic force microscopy (CP-AFM) to image the surfaces of BDD, doped with gas-phase B_2H_6 concentrations of 0−10 ppm, to map the conductive and electrochemically active areas of the surface. These gas-phase concentrations produce diamond films with room-temperature carrier concentrations ranging from 10^{17} to 10^{20} B/cm^3 and carrier mobilities ranging from 2 to 100 cm^2/V·s. All electrochemical experiments were carried out using the outer-sphere redox system $Ru(NH_3)_6^{+3/+2}$, whose heterogeneous rate constant should be largely independent of the nature of the electrode surface.[19,20] Results are presented which show that at low doping levels it is possible to image areas of high conductivity/electrochemical activity, whose density correlates with boron doping level. This suggests that the second model outlined above more accurately describes the nature of electron transfer at the BDD interface at low doping levels, as will be discussed further below.

2. Experimental Section

I. Growth and Preparation of Thin-Film BDD Electrodes. Diamond films of 4 μm thickness were grown by chemical vapor deposition onto conductive p-type silicon wafers using MWCVD and $CH_4/H_2/B_2H_6$ source gas mixtures, as described previously.[4] The concentration of diborane, B_2H_6, in the gas feed mixture was varied to create films of different doping levels. The gas-phase concentrations were 0 ppm (sample #883), 0.5 ppm (sample #900), 1 ppm (sample #908), 5 ppm (sample #922), and 10 ppm (sample #935). The boron doping level of these films ranged from 3×10^{19} to 6×10^{20} cm^{-3}, as determined from boron nuclear reaction analysis (Ion Beam Analysis Laboratory, Case Western Reserve University). The room temperature carrier concentrations and mobilities of these films were approximately 2×10^{17} B/cm^3 and 100 cm^2/V·s (0.1 ppm), 2×10^{17} B/cm^3 and 100 cm^2/V·s (0.5 ppm), 8×10^{17} B/cm^3 and 80 cm^2/V·s (1 ppm), 3×10^{19} B/cm^3 and 30 cm^2/V·s (5 ppm), and 2×10^{20} B/cm^3 and 10 cm^2/V·s (10 ppm), as determined from one set of Hall measurements (NREL). In the "as-grown" condition, all of the films are hydrogen terminated. At the end of the deposition period, the CH_4 and B_2H_6 gas flows were stopped, and the films remained exposed to an H_2 plasma at 1000 W and 45 Torr for an additional 10 min. The plasma power and pressure were then slowly reduced over a 5-min period to cool the samples to a temperature below 400 °C, in the presence of atomic hydrogen. The plasma power was then turned off, and the films were cooled to room temperature under a flow of H_2. The postgrowth annealing in atomic hydrogen served to gasify any adventitious nondiamond sp^2 carbon impurity, to minimize dangling bonds, and to fully hydrogenate the surface. Electrical contact was made to a copper plate, through the bottom of the silicon substrate, by scratching the substrate to remove the oxide layer, cleaning with ethanol, and applying a layer of conducting silver paint. The BDD electrode and the copper plate were clamped in firm contact at the bottom of a cell by means of a rubber O ring.

A great deal of attention was paid to preparing the electrode surfaces for measurement. In the past, our normal protocol for preparing a new diamond electrode for use was to expose the film to a two-part acid-washing procedure prior to rehydrogenating the surface.[20] The first step involved immersing the films in hot aqua regia for 30 min to remove metallic impurities. The films were then rinsed with ultrapure water. The second step involved exposing the samples for 30 min to a warm solution of 30% H_2O_2 to remove nondiamond carbon impurity from the surface. The films were then rinsed with ultrapure water and rehydrogenated to remove the surface oxides formed during the acid washing. We have since gone away from this treatment as we have found that (i) the slow cool-down procedure in atomic hydrogen is sufficient to remove adventitious levels of nondiamond carbon impurity from the surface (i.e., grain boundaries) and (ii) $Ru(NH_3)_6^{+3/+2}$ electron transfer is not mediated by nondiamond carbon impurity at the surface and is largely unaffected by the surface chemistry.[20] The films used in the present work were not subjected to the two-step acid washing.

II. Conductive AFM Measurements. CP-AFM measurements were carried out in air with a Digital Instruments Nanoscope IV AFM equipped with a dual TUNA and CP-AFM imaging module. A Pt-coated silicon tip (MikroMasch NSC14/Pt/15 rectangular cantilever with a radius of curvature less than 35 nm, tip height 15−20 μm, and full tip cone angle less than 20°) was used in the contact mode. The diamond samples were placed on a slide of conducting ITO and contact made between the slide and the sample through the bottom of the conducting silicon by means of colloidal silver paint. The samples were biased at −200 mV relative to the tip. Conducting images could be recorded simultaneously with the topographical images.

III. Cyclic Voltammetry and SECM Measurements. All cyclic voltammetry experiments were carried out using a three-electrode cell, the working electrode being the BDD, held in the bottom of a Teflon cell by means of a rubber O ring (exposed geometric area, 0.283 cm^2) and contact made to the back of the conducting silicon substrate by copper plate, as described above. The counterelectrode was a Pt wire, and Ag/AgCl was used as the reference electrode. For SECM experiments, a 25 or 2 μm diameter Pt wire, sealed in glass and polished to form a tip of RG 10,[22] was used as the working/probe electrode, while the BDD electrode formed the substrate. A CHI 900 potentiostat

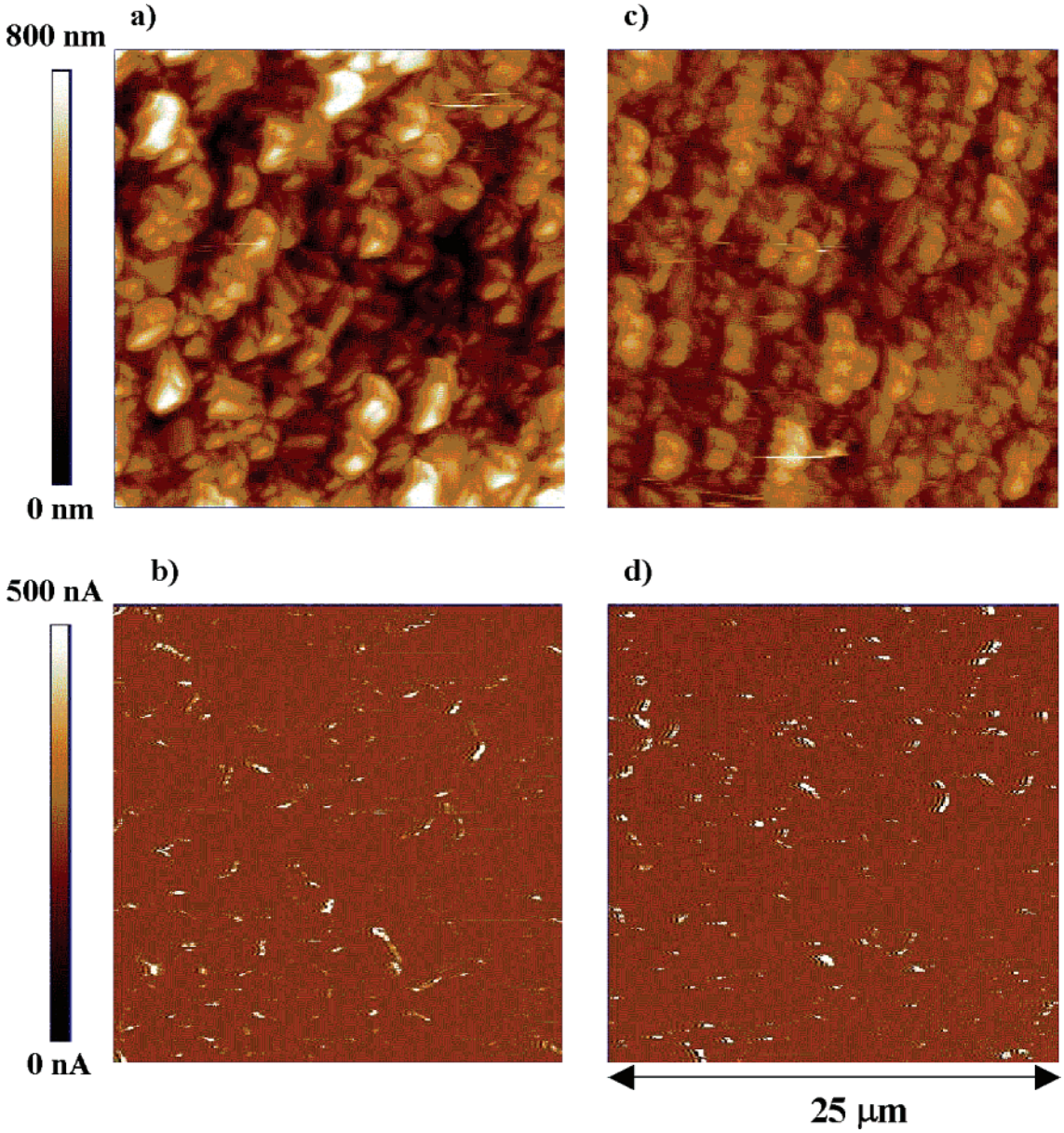

Figure 1. (a) Topographical AFM image of BDD sample doped with 0.5 ppm B_2H_6. (b) Conductive AFM image recorded simultaneously with topographical image (a) of sample doped with 0.5 ppm B_2H_6, with a bias of −200 mV applied between sample and tip. (c) Topographical AFM image of BDD sample doped with 10 ppm B_2H_6. (d) Conductive AFM image recorded simultaneously with topographical image (c) of sample doped with 10 ppm B_2H_6, with a bias of −200 mV applied between sample and tip.

and SECM (CH Instruments, Austin, TX) was used to position the tip and to perform electrochemistry. Approach curves were carried out at 1 μm s^{-1} and images in the $x-y$ plane carried out at different scan rates, described below. In most experiments, 1.3 mM or 5 mM hexaammineruthenium (III) chloride (Strem Chemicals, Newburyport, MA) in 0.1 M KCl (Aldrich) was used as the redox and mediator species and deionized water (Milli-Q, Millipore Corp.) was used for all solutions. Solutions were degassed with argon prior to all experiments.

3. Results and Discussion

I. CP-AFM. CP-AFM uses a conductive tip in the contact mode to measure the conductivity of the diamond surface simultaneously with the surface topography. Figure 1 shows topographical images with the corresponding conductivity images for the sample prepared with 0.5 ppm B_2H_6 (parts a and b of Figure 1) and the sample prepared with 10 ppm B_2H_6 (parts c and d of Figure 1). In both cases, the diamond was biased to −200 mV relative to the tip. The conductivity images show that both samples are insulating over much of the sampled area, with most of the surface recording zero current. The areas of conductivity are of the order of 0.5−2 μm in diameter and are randomly and nonuniformly distributed over the surface. Some of the conductive areas appear to be clustered together at the same location, whereas others appear to be completely isolated. There is some correlation between the topography and the conductivity, with many areas of high conductivity being associated with grain boundaries between diamond crystallites. The size and pattern of distribution of the conductive areas is the same for both samples, but the density of high conductivity sites is higher for the 10 ppm B_2H_6 sample compared to the 0.5 ppm B_2H_6 sample.

The pattern of conductivity observed suggests that the diamond consists of an insulating matrix with sites of high conductivity, which may be associated with the presence of boron dopant in those areas. As electrical contact was made

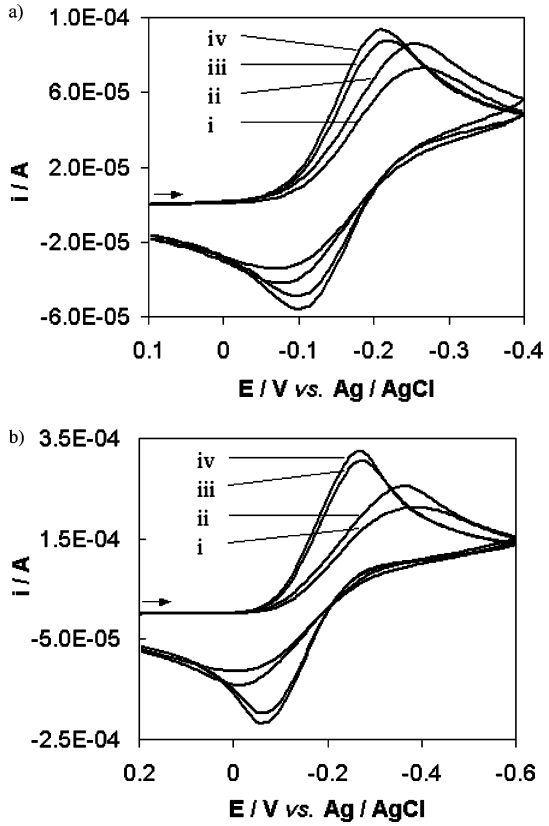

Figure 2. (a) CVs for the reduction of 1.3 mM $Ru(NH_3)_6^{3+}$ in 0.1 M KCl, at scan rate 100 mV s^{-1}, at BDD electrodes (area 0.283 cm^2) doped to: (i) 0.5 ppm, (ii) 1.0 ppm, (iii) 5.0 ppm, and (iv) 10.0 ppm. (b) CVs for the reduction of 5.0 mM $Ru(NH_3)_6^{3+}$ in 0.1 M KCl, at scan rate 100 mV s^{-1}, at BDD electrodes (area 0.283 cm^2) doped to: (i) 0.5 ppm, (ii) 1.0 ppm, (iii) 5.0 ppm, and (iv) 10.0 ppm.

from the bottom of the silicon substrate, this indicates that conduction is only possible along certain pathways through the diamond film from the substrate to the surface. Thus, areas of conductivity may correspond to sites where surface boron dopant sites can establish electrical contact to the silicon substrate through the film. The distribution of dopant on the surface could be greater than that detected by CP-AFM, but many boron sites may be electrically inactive due to a lack of conductive pathways within the film or passivation with H and adventitious N. The dopant is also likely to be nonuniformly distributed within the diamond. Boron doping is said to be heaviest on {111} crystal faces[21] and may tend to concentrate at grain boundaries and defects. There is evidence of this in the images in Figure 1, where some correlation is observed between surface topography and conductivity. High conductivity is observed in the intercrystallite regions, suggesting that boron is present at a high concentration at these sites or that conduction through the film is facilitated by the presence of grain boundaries, perhaps by the presence of sp^2 inclusions or other defects. The density of conducting areas increases as the doping level increases, confirming that these areas are associated with boron sites.

These CP-AFM experiments lend support to the second model of conduction in BDD suggested in the Introduction.

II. Cyclic Voltammetry of the Outer-Sphere $Ru(NH_3)_6^{3+/2+}$ Couple on BDD Electrodes. Figure 2a shows CVs for the reduction of 1.3 mM $Ru(NH_3)_6^{3+}$ in 0.1 M KCl, on BDD samples prepared with 0.5, 1, 5, and 10 ppm B_2H_6 in the source gas mixture. A scan rate of 100 mV s^{-1} was used to record the scans. At this scan rate, the peak currents for reduction (i_p^{red}) and for oxidation (i_p^{ox}) exhibit an increase in value with increasing boron doping level. There is also a decrease in the separation (ΔE_p) between the reduction peak (E_p^{red}) and the oxidation peak (E_p^{ox}) with increasing boron doping level. Figure 2b shows CVs for the reduction of 5 mM $Ru(NH_3)_6^{3+}$ in 0.1 M KCl, on the same BDD samples, also at a scan rate of 100 mV s^{-1}. These CVs exhibit the same relationship between peak height and boron doping level, but in all cases, the peak separations are greater than observed for the same sample in the less concentrated 1.3 mM solution. Table 1 summarizes the values of i_p^{red} and ΔE_p for each sample at 100 mV s^{-1} in 1.3 mM and 5 mM $Ru(NH_3)_6^{3+}$. The lowest value for ΔE_p (112 mV) is obtained for the 10 ppm sample in 1.3 mM $Ru(NH_3)_6^{3+}$, but this value is much larger than the values of 70 mV that can be observed for this redox couple at more highly doped samples.[1] CVs were carried out with the same BDD samples at different scan rates (10−500 mV s^{-1}) in 1.3 and 5 mM $Ru(NH_3)_6^{3+}$ in 0.1 M KCl, where for each sample the peak separations increased with scan rate. Also, in each case the experimental data exhibited a nonlinear relationship between i_p^{red} and $\nu^{1/2}$, where ν is the scan rate, indicating that the outer-sphere reduction of $Ru(NH_3)_6^{3+}$ exhibits non-Nernstian behavior at these BDD electrodes. No corrections for double-layer (Frumkin) effects were applied to these data.

TABLE 1: Table Showing Values of Reduction Peak Height (i_p^{red}) and Peak Separations (ΔE_p) for the Reduction of 1.3 mM and 5.0 mM $Ru(NH_3)_6^{3+}$ in 0.1 M KCl, at Scan Rate 100 mV s^{-1}, at BDD Electrodes (area 0.283 cm^2) at Different Boron-Doping Levels

source gas B_2H_6 level/ppm	concentration $Ru(NH_3)_6^{3+}$/mM	i_p^{red}/mA	ΔE_p/mV
0.5	1.3	0.0744	197
1.0	1.3	0.0861	182
5.0	1.3	0.0877	117
10.0	1.3	0.0934	112
0.5	5.0	0.212	385
1.0	5.0	0.255	367
5.0	5.0	0.305	225
10.0	5.0	0.323	220

An increase in peak separation with increased scan rate can be indicative of two factors: (1) a slow heterogeneous rate constant (k^0) for electron transfer or (2) a large uncompensated resistance (R_u) present within the electrode film. Both factors have the same effect on the shape of the voltammogram and cause the waves to become drawn-out and shifted to higher overpotentials (increased peak separation) and to become flattened (smaller peak currents). It is often very difficult to separate the two factors in the quantitative analysis of CVs. In this case, it is likely that both factors could influence the shape of the voltammograms. Highly doped BDD electrodes typically exhibit some quasireversibility with respect to the $Ru(NH_3)_6^{3+/2+}$ couple, with values of the heterogeneous rate constant, k^0, for this redox couple being reported in the range 0.01−0.1 cm s^{-1} (for 1 M KCl).[1,18] The electron transfer is likely to be slower on the films used in these experiments, as they have a lower doping level. However, the increase in the ΔE_p value as the concentration of redox species is increased from 1.3 to 5 mM indicates a large R_u is also present within the film. Whereas k^0 should be unaffected by solution concentration, the influence of R_u increases with current, so as the concentration of the electroactive species is increased so too is the effect of R_u on the CV.

The CP-AFM data suggests that the electrode surface consists of electrochemically active areas within an insulating, less-active matrix. This can be treated analytically as an ensemble of microelectrodes[23−24] or as an electrode covered by a blocking layer, which has pinholes through which the solution redox

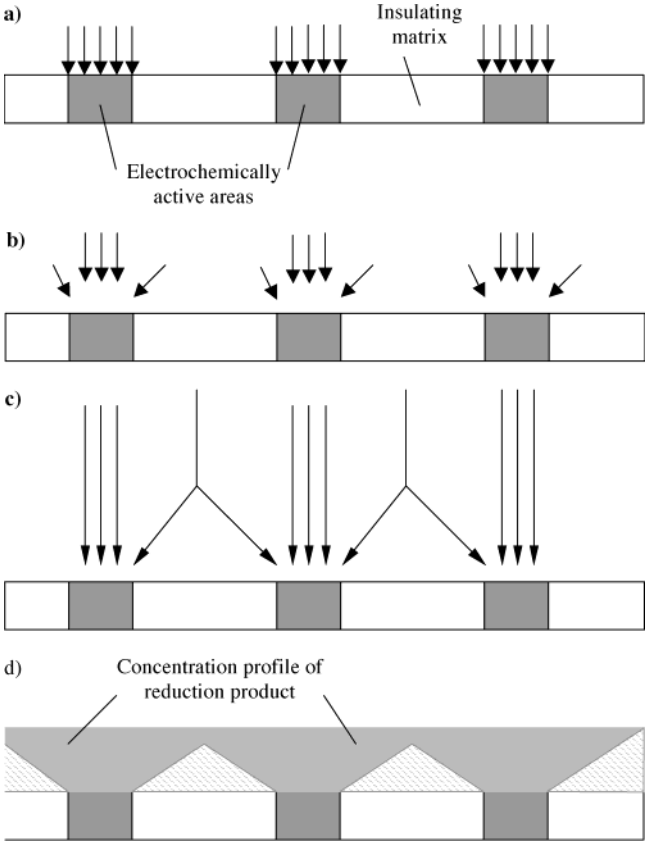

Figure 3. Schematic diagrams to illustrate the diffusion field at an electrode with active (conducting) and inactive (insulating) areas on its surface at (a) short, (b) intermediate, and (c) long time scales, compared to the time-scale of the experiment. (d) Schematic of concentration profile of reduction product, which builds up during the forward scan of CV (light gray areas). Striped areas represent regions above nonactive electrode areas, to where product can diffuse and escape reoxidation during reverse scan.

species can reach the electrode surface.[25−29] The electrochemical response of such an electrode depends on the area of the diffusion field around the electrochemically active areas, which is a function of the size and spacing of the active areas as well as the time scale of the experiment, as illustrated in Figure 3. Figure 3a shows that at short electrolysis times the diffusion layer thickness, δ, is small in comparison to the size of the active areas and so the area of the diffusion field is the sum of the geometric areas of the active spots. At intermediate experimental time scales (Figure 3b), a radial diffusion component is added, as the diffusion fields begin to extend outside the geometric boundaries of the active areas. At longer times (Figure 3c), when δ is thicker than the separation between the active spots, the diffusion fields for each spot merge and linear diffusion is observed, with the diffusion area being equal to the geometric area of the electrode, including the insulating regions. For each BDD electrode, the time regime that dominates will depend on the size and distribution of the active spots (doping level), as well as the concentration of redox species and the scan rate in cyclic voltammetry experiments. Various models and computational techniques have been used to simulate the electrochemical response of such electrodes, as a function of coverage of active electrode area, size of active spots, and spot distribution, in the fast, slow, and intermediate time regimes.[23−29] In general, depending on the active area coverage, at fast and intermediate times the apparent heterogeneous rate constant, k_{eff}, is found to be slower than the heterogeneous rate constant for a 100% active surface, k^0, and is given by

$$k_{\text{eff}} = k^0(1 - \theta) \quad (1)$$

where θ is the coverage of blocked (inactive) area. However, the exact form of the CVs obtained depends on many factors such as redox species, concentration, active site size, and spacing and requires simulation on a case-by-case basis.

The rate constants for quasireversible reactions are typically extracted from CVs using the Nicholson method.[30] However, this method does not allow for the deconvolution of the effect of slow heterogeneous kinetics and uncompensated resistance. For this reason, in this case, experimental CVs were fitted using the *DigiSim 3.03* program (Bioanalytical Systems Ltd.), where experimental data can be simulated as a function of heterogeneous rate constant, k^0, and uncompensated resistance, R_u. *DigiSim* simulations assume semi-infinite linear diffusion, such as what would be observed for long time regimes, as illustrated in Figure 3c. By fitting the experimental CVs in this way, we assumed that the experiments were carried out at a slow enough time scale that diffusion to each active spot is linear and semi-infinite and that the diffusion area will be equal to the geometric area of the electrode. This is a reasonable assumption for the CVs carried out at the relatively slow scan rates of 10−500 mV s^{-1}. Thus CVs for these BDD electrodes can be simulated using this model, and deviations between the simulation and experimental voltammograms will give information on the nature of the diffusion field and the electrochemically active area of the electrode. As the electrochemically active areas become more sparsely distributed, this model can no longer be assumed and the experimental CVs may represent the intermediate or fast time scales and so can no longer be fitted using these simulations.

Figure 4a shows the experimental data (black) and the simulated data (gray) for the reduction of 1.3 mM $Ru(NH_3)_6^{3+}$ at the 10 ppm B_2H_6 BDD electrode, at scan rates of 10, 20, 50, and 100 mV s^{-1}. The data have been fit assuming a semi-infinite linear diffusion to an electrode of area 0.283 cm^2 (geometric area) and the diffusion coefficient, D, for $Ru(NH_3)_6^{3+}$ and $Ru(NH_3)_6^{2+}$ was taken as 1×10^{-5} cm^2 s^{-1} (the actual value is probably closer to 0.53×10^{-5} cm^2 s^{-1}, but the assumed value is sufficient for the analysis presented). The simulation gives a value for uncompensated resistance, R_u, of 150 Ω and for heterogeneous rate constant, k^0, of 0.012 cm s^{-1}. This value of k^0 is consistent with values obtained for highly doped BDD samples in the literature.[1] That these same parameters fit the experimental data obtained for the 10 ppm sample with 5 mM $Ru(NH_3)_6^{3+}$ lends some confidence to these values. As can be seen in parts a and b of Figure 4, the simulated data fits the experimental data very well on the forward scan but on the reverse scan, although the position of the peak is correct, the values of simulated current are consistently 5−10% higher than those obtained by experiment. This can be explained by considering the concentration profile of the $Ru(NH_3)_6^{2+}$ species generated at the electrochemically active areas during the forward scan, as shown in Figure 3d. The gray shaded areas in the figure illustrate where the concentration of $Ru(NH_3)_6^{2+}$ builds up and where the diffusion fields around each active site begin to overlap. However, before the reverse scan occurs this species can diffuse to regions above the inactive electrode area (striped in the Figure) and so are less available for oxidation during the reverse scan. Hence the oxidation peak current is always less than the reduction peak current value when there is a hemispherical diffusion element. Similar problems have been encountered in attempting to fit both forward and backward experimental CV peaks to the same parameters in different

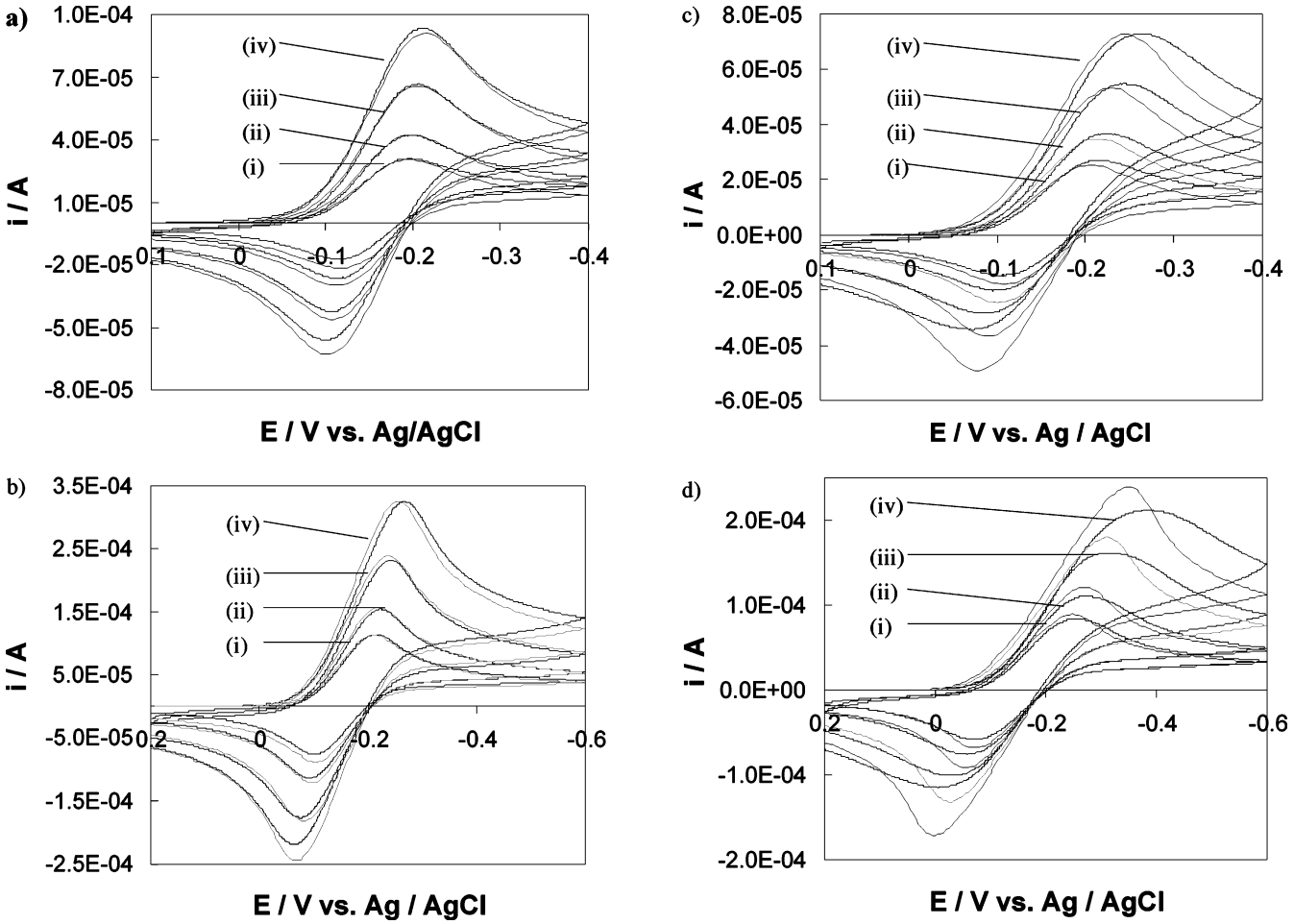

Figure 4. Experimental (black lines) and *DigiSim*-simulated (grey lines) CVs for the reduction of $Ru(NH_3)_6^{3+}$ in 0.1 M KCl at BDD electrodes (geometric area 0.283 cm^2) at (i) 10, (ii) 20, (iii) 50, (iv) 100 mVs^{-1}. (a) 1.3 mM $Ru(NH_3)_6^{3+}$ at 10 ppm doped electrode, simulated with $k^0 = 0.012$ cm s^{-1}, $R_u = 150\ \Omega$, $A = 0.283$ cm^2. (b) 5 mM $Ru(NH_3)_6^{3+}$ at 10 ppm doped electrode, simulated with $k^0 = 0.012$ cm s^{-1}, $R_u = 150\ \Omega$, $A = 0.283$ cm^2. (c) 1.3 mM $Ru(NH_3)_6^{3+}$ at 0.5 ppm doped electrode, simulated with $k^0 = 0.012$ cm s^{-1}, $R_u = 550\ \Omega$, $A = 0.240$ cm^2. (d) 5 mM $Ru(NH_3)_6^{3+}$ at 0.5 ppm doped electrode, simulated with $k^0 = 0.012$ cm s^{-1}, $R_u = 550\ \Omega$, $A = 0.240$ cm^2.

simulation strategies.[26,29] This analysis shows that although the electrode may consist of discrete areas of conductivity, at the scan rates used in the experiment, the diffusion area is equal to the geometric area of the electrode, and so little difference is observed in the CVs between this electrode and one of the same geometric area which has uniform conductivity. In fact, the rate constant obtained is comparable to that of a highly doped film, the only influence on the CV appears to be the existence of resistance through the film.

Parts c and d of Figure 4 show experimental CVs (black) and simulated CVs (grey) for the reduction of 1.3 mM (Figure 4c) and 5 mM (Figure 4d) $Ru(NH_3)_6^{3+}$ at the 0.5 ppm B_2H_6 BDD electrode, at scan rates of 10, 20, 50, and 100 mV s^{-1}. By use of the same geometric area as the 10 ppm sample (0.283 cm^2), it was not possible to obtain a good fit for the experimental data in this case. The best fit using this model was to use a value of 0.240 cm^2 for the geometric area, values of 1×10^{-5} cm s^{-2} for the diffusion coefficients, and $R_u = 550\ \Omega$ and $k^0 = 0.012$ cm s^{-1}. As can be seen in the figure, the fit is very poor, the values of R_u and k^0 giving approximately correct peak positions and peak currents but with large deviations with respect to the shape of the peaks. The large value of R_u suggests that the film is much less conductive than the more highly doped 10 ppm sample. There are no values of R_u and k^0 that fit the experimental data using the geometric area value of 0.283 cm^2. This suggests that the electrochemically active area of the electrode is considerably smaller than the geometric area and that the linear diffusion model as illustrated in Figure 3c cannot be assumed in this case. The electrochemically active areas are small enough and distributed far enough apart for the CVs to be taking place in the intermediate time regime as illustrated in Figure 3b. In this case, it will not be possible to fit these CVs using the *DigiSim* approach and instead a simulation assuming a contribution from radial diffusion[27] would be required.

In general, the CVs for these BDD samples support the model that the surface consists of discrete electrochemically active areas in an insulating matrix. The most highly doped film, prepared with 10 ppm B_2H_6, shows a value of k^0 that is consistent with literature values, but the increased peak separation is due to a relatively high resistance in the film. The simulated CV fits the experimental data very well on the forward scan, showing that under these experimental conditions diffusion can be assumed to be linear and semi-infinite and therefore that spacing between active spots is very small in comparison to the diffusion layer thickness. The lowest doped film (0.5 ppm B_2H_6) shows deviations from this model and also exhibits considerably greater resistance. The simulations show that reduction of $Ru(NH_3)_6^{3+}$ can be assumed to take place on more sparsely distributed active spots with the same value of k^0 as on the more highly doped sample, but from the geometric areas used to fit the CVs, the electrochemically active area is at least 20% smaller.

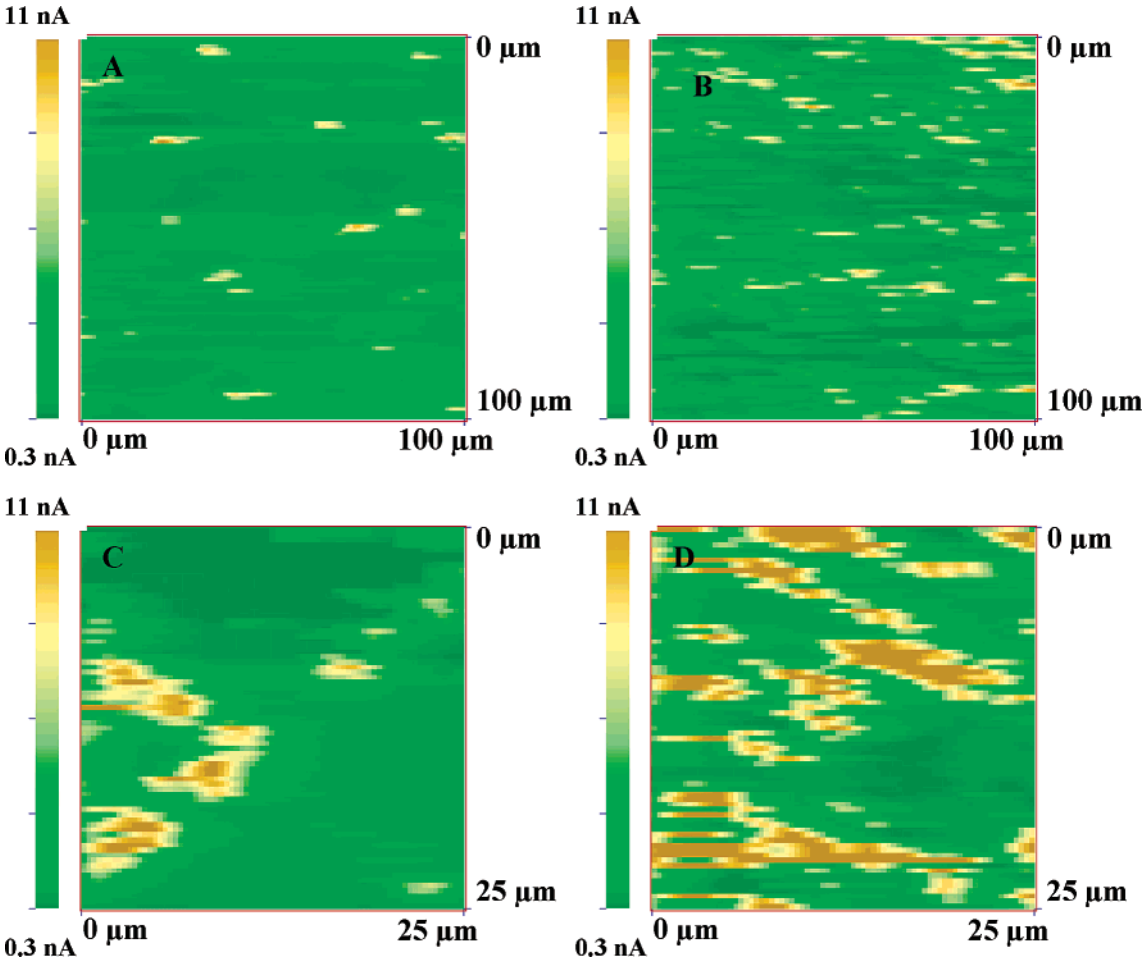

Figure 5. SECM images of BDD substrates obtained with a 2 μm Pt tip in 1.3 mM $Ru(NH_3)_6^{3+}$ in 0.1 M KCl, with tip potential −0.4 V vs Ag/AgCl and substrate potential 0 V vs Ag/AgCl, tip−substrate separation 1−2 μm: (a) 0.5 ppm doped BDD, scan rate 30 μm s^{-1}; (b) 10 ppm doped BDD, scan rate 30 μm s^{-1}, (c) 0.5 ppm doped BDD, scan rate 10 μm s^{-1}; (d) 10 ppm doped BDD, scan rate 10 μm s^{-1}.

III. SECM Images of the Boron-Doped Diamond Substrates. SECM makes use of an ultramicroelectrode (UME) tip to approach to within a few micrometers of a substrate and probe the electrochemical activity at the surface. Typically the tip potential is chosen to oxidize or reduce a mediator species in solution at steady state, and the change in the tip current is monitored as the tip approaches to within a few tip radii of the substrate. A plot of the experimental tip current vs tip−substrate separation is called an approach curve and can give information about the nature of the substrate. Approach to an insulating surface typically results in negative feedback, where diffusion of fresh mediator species to the tip is blocked as it moves within a few tip radii of the substrate and the current rapidly drops to zero as the tip touches the surface. If the substrate is a conductor, its potential can be selected so that it reoxidizes or rereduces the species being produced at the tip. In this case, as the tip approaches the surface, positive feedback results and an increase in current is observed. Experimental curves can be compared to theory in order to accurately determine the height of the tip above the substrate surface. By use of the SECM in imaging mode, it is possible to scan over the substrate in the $x-y$ plane at a fixed height above the surface and obtain an image of the feedback. This allows areas of high electrochemical activity to be mapped out.

Parts a and b of Figure 5 show images obtained when a 2 μm diameter Pt tip is scanned at 30 μm s^{-1} in the $x-y$ plane approximately 1−2 μm above the (a) 0.5 ppm and (b) 10 ppm B_2H_6 films, over a 100 μm × 100 μm area. The mediator in this case was 1.3 mM $Ru(NH_3)_6^{3+}$ in 0.1 M KCl. The tip potential was −0.4 V vs Ag/AgCl, and the substrate potential was 0 V. Under these conditions, a conducting substrate should exhibit positive feedback as the tip approaches a distance within a few tip radii, due to the reoxidation of the tip product at the substrate. The positive feedback phenomenon is illustrated schematically in Figure 6a. The images in Figure 5 show substrates of nonuniform electrochemical activity, with currents ranging from 0.3 nA, indicating negative feedback, to ∼11 nA indicating positive feedback. (Steady-state current at $i_{T,\infty}$ for a 2-μm tip in 1.3 mM $Ru(NH_3)_6^{3+}$ is 0.45 nA). The areas of negative feedback indicate no electrochemical activity in the substrate. The areas of positive feedback indicate conducting areas in the film. The 10 ppm B_2H_6 diamond shows a greater density of electrochemically active sites in comparison to the 0.5 ppm B_2H_6 sample. For both samples, the sites are randomly and nonuniformly distributed. The slight streakiness to the images is due to minor hysteresis in the motion of the inchworms that drive the SECM stage in the x direction, which can be removed to some extent by careful calibration.

To obtain higher resolution images, scans were carried out over smaller 25 μm × 25 μm areas at a slower scan rate of 10 μm s^{-1}, as shown in Figure 5 for (c) 0.5 ppm and (d) 10 ppm. Again, the surfaces show nonuniform activity with currents in the range 0.3 nA (negative feedback) to 11 nA (positive feedback). This indicates a largely insulating surface, with conductive areas of the order of 1−5 μm in diameter exhibiting a high electrochemical activity. These areas are spaced between

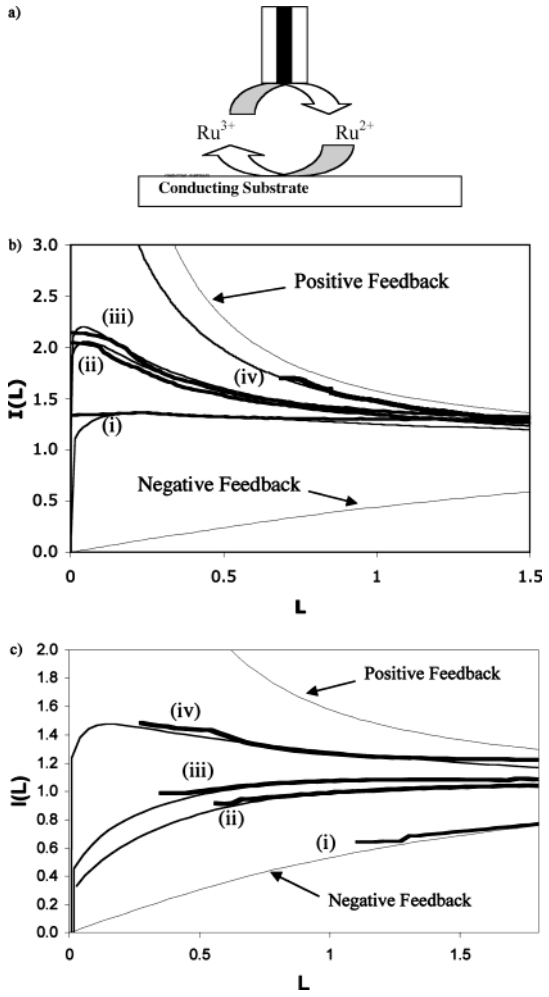

Figure 6. (a) Schematic diagram illustrating positive feedback at a conductive substrate. (b) Experimental approach curves (thick black lines) obtained with a 25 μm diameter Pt tip approaching BDD substrates, in 1.3 mM $Ru(NH_3)_6^{3+}$ in 0.1 M KCl, with tip potential -0.4 V vs Ag/AgCl and substrate potential 0 V vs Ag/AgCl, for: (i) 0.5, (ii) 1, (iii) 5, and (iv) 10 ppm doped BDD. Theoretical curves (gray lines) are calculated from eq 3 using values of (i) $k_{eff} = 0.010$ cm s^{-1}, (ii) $k_{eff} = 0.019$ cm s^{-1}, (iii) $k_{eff} = 0.021$ cm s^{-1}, (iv) $k_{eff} = 0.072$ cm s^{-1}. Thin black lines show approach curves predicted for pure positive and negative feedback, calculated from eqs 5 and 4, respectively. (c) Experimental approach curves (thick black lines) obtained with a 2 μm diameter Pt tip approaching BDD substrates, in 1.3 mM $Ru(NH_3)_6^{3+}$ in 0.1 M KCl, with tip potential -0.4 V vs Ag/AgCl and substrate potential 0 V vs Ag/AgCl, for: (i) 0.5, (ii) 1, (iii) 5, and (iv) 10 ppm doped BDD. Theoretical curves (grey lines) are calculated from eq 3 using values of (ii) $k_{eff} = 0.033$ cm s^{-1}, (iii) $k_{eff} = 0.050$ cm s^{-1}, (iv) $k_{eff} = 0.150$ cm s^{-1}. Curve (i) was fit to the expression for negative feedback. Thin black lines show approach curves predicted for pure positive and negative feedback, calculated from eqs 5 and 4, respectively.

1 and 25 μm apart. These electrochemical "hot-spots" correspond well to the regions of high conductivity observed using CP-AFM. When the 2 μm tip is positioned over one of these sites and an approach curve obtained, positive feedback can be observed. Again the 10 ppm sample shows a greater density of such sites, confirming the correlation between the doping level and electrochemically active electrode area. Taking parts c and d of Figure 5 as representative for the 0.5 and 10 ppm samples, approximate values can be estimated for the electrochemically active area of the electrodes. Figure 5a suggests that less than 25% of the 0.5 ppm electrode is electrochemically active, whereas Figure 5b shows that a much larger area of the 10 ppm electrode is active, up to 50%, and as the CV data showed, the active areas are located close enough together so that the CV response is the same as for an electrode with 100% active area.

SECM imaging, therefore, confirms that the entire electrode area is not electrochemically active, consistent with CP-AFM and CV results, for a boron-doped diamond electrode prepared with B_2H_6 levels of less than 10 ppm. This proves that a model close to the second described in the Introduction most accurately describes the mechanism of electron transfer at the diamond/solution interface for BDD at these doping levels. The sites where electron transfer takes place may be where there is an accumulation of boron dopant or where conducting pathways are available through the diamond film. At higher dopant levels than used in this work, the mechanism of electron transfer may differ, as interaction between neighboring boron sites becomes more important. This may lead to more uniform activity of the electrode surface and an electrochemically active surface that is more comparable to the geometric area.

IV. SECM Approach Curves at the Diamond Substrates. Approach (i_T-d) curves were recorded in the feedback mode in a 1.3 mM solution of $Ru(NH_3)_6^{3+}$ in 0.1 M KCl using a 25 μm diameter Pt tip held at a potential of -0.4 V vs Ag/AgCl, over a diamond substrate held at a potential of 0 V vs Ag/AgCl. With this relatively large Pt disk diameter, the tip samples both conducting and insulating portions of the surface simultaneously. Figure 6b shows experimental approach curves (thick black lines) obtained using a 25 μm Pt tip for approach to the 0.5, 1, 5, and 10 ppm B_2H_6 diamond substrates, along with the curves theoretically predicted for diffusion-controlled positive feedback for approach to a conductor and negative feedback for approach to an insulator (thin black lines). In each case, the normalized current $I(L) = i_{lim}/i_\infty$ has been plotted against normalized distance from the substrate, $L = d/a$, where i_∞ is the steady-state limiting current of the tip far removed from the substrate and a is the radius of the electrode. The figure shows that approach to the 10 ppm B_2H_6 sample results in positive feedback and the experimental data points almost follow the theoretical curve for pure positive feedback, indicating that the surface is conducting, with fast heterogeneous kinetics at this potential. Behavior close to pure positive feedback was observed for this sample regardless of lateral position of the tip on the substrate. In contrast, the 5, 1, and 0.5 ppm B_2H_6 samples show behavior indicative of kinetically limited positive feedback. The tip current initially shows a rise in current due to positive feedback, which then falls to lower values as the tip continues to approach the surface. Such behavior is characteristic of surfaces where heterogeneous kinetics are finite. The approach curves for these samples were very dependent on the lateral position of the tip above the substrate and approach over different areas resulted in varying degrees of positive feedback, because, as discussed previously, the conductivity is not uniform over the diamond surface. This was especially true of the 5 ppm B_2H_6 substrate, where sometimes diffusion-controlled positive feedback could be observed, similar to the 10 ppm sample.

The analysis of SECM approach curves to a nonuniformly conductive or partially blocked surface has been discussed, using the example of a gold substrate partially blocked with a self-assembled monolayer.[31] The steady-state diffusion-limited current to a uniformly accessible surface partly covered by randomly distributed active disks was shown to be equivalent to the kinetically controlled current at the same surface but with an effective rate constant

$$k_{eff} = 4(1 - \theta)D/\pi R_d \qquad (2)$$

TABLE 2: Values of Apparent Heterogeneous Rate Constant, k_{eff}, and Coverage of Electrochemically Active Area ($1 - \theta$), Calculated from Eqs 2 and 3 by Fitting Approach Curves in Figure 6 for BDD Substrates of Different Doping Levels

source gas B_2H_6 level/ppm	tip radius/μm	k_{eff}/cm s^{-1}	($1 - \theta$) coverage of electrochemically active area
10	12.5	0.072	0.57
5	12.5	0.021	0.17
1	12.5	0.019	0.14
0.5	12.5	0.01	0.08

where θ is the fraction of the surface that is insulating and R_d is the radius of the conductive areas. Thus, the SECM approach curve at a partially conductive substrate should have the same shape as the kinetically controlled i_T-d curve at a completely conductive substrate where the heterogeneous kinetics are finite. This can be described by eq 3[32]

$$I_T^{K}(L) = I_S(1 - I_T^{INS}/I_T^{C}) + I_T^{INS} \quad (3)$$

where I_T^C, I_T^K, and I_T^{INS} represent the tip current for the diffusion-controlled regeneration of a redox mediator, finite substrate kinetics, and insulating substrate, respectively, given by the analytical approximations

$$I_T^{INS} = 1/[0.292 + 1.5151/L + 0.6553\exp(-2.4035/L)] \quad (4)$$

$$I_T^{C} = 0.68 + 0.78377/L + 0.3315\exp(-1.0672/L) \quad (5)$$

$$I_S = 0.78377/L(1 + 1/\Lambda) + [0.68 + 0.3315\exp(-1.0672/L)]/[1 + F(L,\Lambda)] \quad (6)$$

where $F(L,\Lambda) = (11/\Lambda + 7.3)/(110 - 40L)$ with $\Lambda = k_{eff}aL/D$, where k_{eff} is the apparent heterogeneous rate constant (cm s^{-1}), as defined in eq 2, and D is the diffusion coefficient of the redox mediator (cm^2 s^{-1}).

The experimental approach curves in Figure 6 have been fit to SECM theory using eq 3 (gray lines), and the resulting values of k_{eff} for each substrate are presented in Table 2. The values range from 0.072 cm s^{-1}, at the more highly doped sample, to 0.010 cm s^{-1} at the sample with the lowest doping level. Using a value of $D = 1 \times 10^{-5}$ cm^2 s^{-1} and estimating an average value of $R_d = 1.0$ μm from the SECM images in Figure 5, approximate values of ($1 - \theta$), the fraction of the area of the diamond substrates that is conductive, can be calculated. The above equations were derived for a uniform array of well-defined spots, as opposed the random array on the BDD electrodes. Nevertheless, the calculated values suggest that approximately 57% of the surface area of the most highly doped sample is conducting and only about 8% of the sample doped to 0.5 ppm is electrochemically active. These values are in broad agreement with the SECM images presented in Figure 5.

Further approach curves were recorded in the feedback mode using a 1.3 mM solution of $Ru(NH_3)_6^{3+}$ in 0.1 M KCl as the mediator species with a 2 μm Pt tip. Because this tip radius is smaller, the tip current samples a much smaller area of the diamond substrate surface than the 25 μm tip. Figure 6c shows a selection of experimental approach curves obtained for approach to the 10, 5, 1, and 0.5 ppm B_2H_6 samples (thick black lines) along with the theoretical curves for pure negative and positive feedback (thin black lines). The figure shows that approach to the sample prepared with 0.5 ppm B_2H_6 typically shows pure negative feedback, which fits almost exactly to theory; however, in some cases as the tip position is changed, some positive feedback can be obtained for this substrate. If the tip approaches the surface directly above an electrochemically active spot as seen on the SECM images in Figure 5, pure diffusion-controlled positive feedback is observed that can be fit to eq 5. This indicates that at the conducting areas electron transfer occurs with fast kinetics. The experimental approach curves to different positions on the 1, 5, and 10 ppm B_2H_6 diamond substrates exhibit a mixture of negative and positive feedback depending on the lateral position of the tip above the surface, indicative of the nonuniform nature of the substrate conductivity. Neither pure negative nor positive feedback is typically observed.

4. Conclusion

CV, CP-AFM, and SECM were used to investigate the nature of electron transfer at BDD samples, with low doping levels of less than 10 ppm. The reduction peak heights in CV were found to depend on the boron-doping level, but differences in peak separations were attributed to uncompensated resistance in the diamond films, rather than slow heterogeneous kinetics. *DigiSim* simulations suggested that the lowest doped samples could not be fit using a semi-infinite linear diffusion model, as the surface consisted of well-spaced electroactive areas within an insulating matrix, where there was some radial component to the diffusion. CP-AFM and SECM imaging showed that the films consisted of predominantly insulating, nonelectrochemically active areas containing isolated sites of very high conductivity and electrochemical activity. These sites were probably below 1 μm in diameter and distributed across the surface. The distribution may be random, although some images (e.g., Figure 5) suggest that the conductive sites are at grain boundaries. The density of these sites increased with boron doping level. SECM approach curves to the different substrates allowed values of the effective heterogeneous rate constants and surface coverage of active sites to be calculated. These results suggest that at low doping levels the diamond surface only has limited sites (~10−60% of the geometric area) where electrochemistry can take place, with electron transfer being reversible at those sites. Redox processes are limited by the availability of such sites rather than by slow heterogeneous rate constants for electron transfer caused by limited migration of carriers to the electrode interface. At higher boron-doping levels, the mechanism of charge transfer may differ, as well as using a different redox species, with a different formal potential relative to the valence band potential of BDD.

Acknowledgment. K.B.H. would like to greatly acknowledge the Robert A. Welch Foundation for partial support of this research. G.M.S. acknowledges the generous support by the Department of Energy, Office of Basic Science (DE-FG02-01ER15120). The authors also thank Dr. David Young (NREL) for the Hall measurements of the diamond film carrier concentration and mobility, Dr. Alan McIlwain (CWRU) for the nuclear reaction measurements to determine the diamond film boron doping levels, and Timothy Smith and Dr. Keith Stevenson (UT Austin) for use of the CP-AFM and technical assistance with measurements.

References and Notes

(1) Granger, M. C.; Witek, M.; Xu, J.; Wang, J.; Hupert, M.; Hanks, A.; Koppang, M. D.; Butler, J. E.; Lucazeau, G.; Mermoux, M.; Strojek, J. W.; Swain, G. M. *Anal. Chem.* **2000**, *72*, 3793.

(2) Compton, R. G.; Foord, J. S.; Marken, F. *Electroanal.* **2003**, *15* (17), 1349.

(3) Tenne, R.; Levy-Clement, C. *Isr. J. Chem.* **1998**, *38* (1−2), 57.

(4) Granger, M. C.; Xu, J.; Strojek, J. W.; Swain, G. M. *Anal. Chim. Acta* **1999**, *397*, (1−3), 145.
(5) Fujishima, A.; Rao, T. N.; Popa, E.; Sarada, B. V.; Tagi, I.; Tryk, D. A. *J. Electroanal. Chem.* **1999**, *473* (1−2) 179.
(6) Rao, T. N.; Sarada, B. V.; Tryk, D. A.; Fujishima, A. *J. Electroanal. Chem.* **2000**, *491* (1−2), 175.
(7) Prado, C.; Murcott, G. G.; Marken, F.; Foord, J. S.; Compton, R. G. *Electroanal.* **2002**, *14* (14), 975.
(8) Troster, I.; Fryda, M.; Herrmann, D.; Schafer, L.; Hanni, W.; Perret, A.; Blaschk, M.; Kraft, A.; Stadelmann, M. *Diamond and Relat. Mater.* **2002** *11* (3−6), 640.
(9) Iniesta, J.; Michaud, P. A.; Panizza, M.; Cerisola, G.; Aldaz, A.; Comninellis, C. *Electrochim. Acta* **2001**, *46* (23), 3573.
(10) Swain, G. M.; Anderson, A.; Angus, J. R. *MRS Bull.* **1998**, *23*, 56.
(11) Ferreira, N. G.; Silva, L. L. G.; Corat, E. J.; Trava-Airoldi, V. J. *Diamond Relat. Mater.* **2002**, *11*, 1523.
(12) Levy-Clement, C.; Zenia, F.; Awa Ndao, N.; Deneuville, A. *New Diamond Frontier Carbon Technol.* **1999**, *9*, 189.
(13) Becker, D.; Juttner, K. *J. Appl. Electrochem.* **2003**, *33*, 959.
(14) Becker, D.; Juttner, K. *Electrochim. Acta* **2003**, *49* (1) 29.
(15) Friso, F.; Trasatti, S. *Collect. Czech Chem. Commun.* **2003**, *68*, 1621.
(16) Ferro, S.; De Battisti, A. *Electrochim. Acta* **2002**, *47*, 1641.
(17) Van de Lagemaat, J.; Vanmaekelbergh, D.; Kelly, J. J. *J. Electroanal. Chem.* **1999**, *475*, 139.
(18) Fisher, A. E.; Show, Y.; Swain, G. M. *Anal. Chem.* **2004**, *76*, 2553.
(19) Chen, P.; McCreery, R. L. *Anal. Chem.* **1996**, *68*, 3958.
(20) Granger, M. C.; Swain, G. M. *J. Electrochem. Soc.* **1999**, *146*, 4551.
(21) Kolber, T.; Piplits, K.; Haubner, R.; Hutter, H. *Fresenius' J. Anal. Chem.* **1999**, *365*, 636.
(22) Bard, A. J.; Fan, F.-R. F.; Mirkin, M. V. In *Electroanalytical Chemistry*; Bard, A. J., Ed.; Marcel Dekker: New York, 1994; pp 243−37, Vol. 18.
(23) Reller, H.; Kirowa-Eisner, E.; Gileadi, E. *J. Electroanal. Chem.* **1982**, *138*, 65.
(24) Reller, H.; Kirowa-Eisner, E.; Gileadi, E. *J. Electroanal. Chem.* **1984**, *161*, 247.
(25) Gueshi, T.; Tokuda, K.; Matsuda, H. *J. Electroanal. Chem.* **1978**, *89*, 247.
(26) Gueshi, T.; Tokuda, K.; Matsuda, H. *J. Electroanal. Chem.* **1979**, *101*, 29.
(27) Amatore, C.; Saveant, J. M.; Tessier, D. *J. Electroanal. Chem.* **1983**, *147*, 39.
(28) Brookes, B. A.; Davies, T. J.; Fisher, A. C.; Evans, R. G.; Wilkins, S. J.; Yunus, K.; Wadhawan, J. D.; Compton, R. G. *J. Phys. Chem. B* **2003**, *107*, 1616.
(29) Davies, T. J.; Brookes, B. A.; Fisher, A. C.; Yunus, K.; Wilkins, S. J.; Greene, P. R.; Wadhawan, J. D.; Compton, R. G. *J. Phys. Chem. B* **2003**, *107*, 6431.
(30) Nicholson, R. S. *Anal. Chem.* **1965**, *37*, 1351.
(31) Forouzan, F.; Bard, A. J.; Mirkin, M. V. *Isr. J. Chem.* **1997**, *37*, 155.
(32) Wei, C.; Bard, A. J.; Mirkin, M. V. *J. Phys. Chem.* **1995**, *99*, 16033.